D–π–A System Based on Zinc Porphyrin Dyes for Dye-Sensitized Solar Cells: Combined Experimental and DFT–TDDFT Study

ARTICLE *in* POLYHEDRON · SEPTEMBER 2015

Impact Factor: 2.01 · DOI: 10.1016/j.poly.2015.08.035

9 AUTHORS, INCLUDING:

Giribabu Lingamallu

Indian Institute of Chemical Technology

134 PUBLICATIONS **2,224** CITATIONS

SEE PROFILE

Senthilarasu Sundaram

University of Exeter

64 PUBLICATIONS **751** CITATIONS

SEE PROFILE

Smagul Karazhanov

Institute for Energy Technology

85 PUBLICATIONS **681** CITATIONS

SEE PROFILE

Tapas K Mallick

University of Exeter

157 PUBLICATIONS **917** CITATIONS

SEE PROFILE

Polyhedron 100 (2015) 313–320

Contents lists available at ScienceDirect

Polyhedron

journal homepage: www.elsevier.com/locate/poly

D–π–A system based on zinc porphyrin dyes for dye-sensitized solar cells: Combined experimental and DFT–TDDFT study

Vamsi K. Narra [a], Habib Ullah [b], Varun K. Singh [a], Lingamallu Giribabu [a,*], S. Senthilarasu [b,*], S.Zh. Karazhanov [c], Asif A. Tahir [b], Tapas K. Mallick [b], Hari M. Upadhyaya [d]

[a] Inorganic and Physical Chemistry Division, Indian Institute of Chemical Technology, Hyderabad 500 007, India
[b] Environment and Sustainability Institute (ESI), University of Exeter, Penryn Campus, TR10 9FE, UK
[c] Department for Solar Energy, Institute for Energy Technology, 2027 Kjeller, Norway
[d] Wolfson Centre for Materials Processing, Institute of Materials and Manufacturing, Department of Mechanical, Aerospace and Civil Engineering, Brunel University, Uxbridge, UB8 3PH London, UK

ARTICLE INFO

Article history:
Received 4 July 2015
Accepted 26 August 2015
Available online 1 September 2015

Keywords:
Porphyrin
Furan
Redox electrolyte
Solar cells
DFT

ABSTRACT

A series of four new porphyrin-furan dyads were designed and synthesized by having anchoring group either at *meso*-phenyl or pyrrole-β position of a zinc porphyrin based on donor–π–acceptor (D–π–A) approach. The porphyrin macrocycle acts as donor, furan hetero cycle acts as π-spacer and either cyanoacetic acid or malonic acid group acts as acceptor. These dyads were fully characterized by UV–Visible, ^{1}H NMR, MALDI-MS and fluorescence spectroscopies and cyclic voltammetry. Both of the observed and TD-DFT simulated UV–Vis spectra has strong correlation which validate and confirm the synthesized dyads and theoretical method for this type of compounds. Both soret and Q-bands are red shifted in the case of pyrrole-β substituted dyads. The redox potentials of all four dyads are not altered in comparison with their individual constituents. The dyads were tested in dye sensitized solar cells and found pyrrole-β substituted zinc porphyrins are showing better performance in comparison with the corresponding *meso*-phenyl dyads. Optical band gap, Natural bonding, and Molecular bonding orbital (HOMO–LUMO) analysis are in favour of pyrrole-β substituted zinc porphyrins contrast to *meso*-phenyl dyads.

1. Introduction

Porphyrins and their derivatives have been intensively studied for many years because of their importance in the photochemistry and photo-biology processes [1–3]. Under the influence of the large planar π-conjugated structure, porphyrin derivatives exhibit good thermal stability, strong two-photon absorption [4], efficient electron transfer [5–7], and interesting photo-electrochemical properties [8]. Therefore, porphyrins have been frequently employed in various fields such as biomimetic natural photosynthesis [9–11], chemical and biological sensors [12], organic light-emitting diodes [13], field effect transistors [14], non-linear optical properties [15] and dye-sensitized solar cells (DSSCs) [16,17].

DSSCs have emerged as an innovative solar energy conversion technology which provides a pathway for the development of low-cost, renewable and environmentally acceptable energy production [18–20]. However, the technology is not yet commercialized due to several technical problems. The sensitizer is one of the key components in achieving high conversion efficiency and durability of the devices. The widely used sensitizers are Ru(II) polypyridyl complexes with a certified conversion efficiency of 11.4% [18,21,22]. In spite of this, the main drawbacks of these sensitizers are the lack of absorption in the red region of the visible spectrum and also relatively low molar extinction coefficient above 600 nm. In this regard, porphyrins and their derivatives are found to be alternative sensitizers to Ru(II) polypyridyl complexes based on their absorption and thermal properties.

Some metalloporphyrins have been tested for the photosensitization of wideband-gap semiconductors, the most common being either free-base or its zinc derivative of the *meso*-benzoic acid substituted porphyrins [23–25]. However, the efficiency of *meso*-substituted porphyrins remained around 3% for a long time till 2007. In order to further improve the efficiency and durability of porphyrin based DSSC devices, one has to tune photophysical properties of porphyrin macrocycle by introducing substituents either at *meso*-phenylor at pyrrole-β position/s. Officer and co-workers have reported a combination of conjugated ethenyl

* Corresponding authors.
E-mail address: S.Sundaram@exeter.ac.uk (S. Senthilarasu).

http://dx.doi.org/10.1016/j.poly.2015.08.035
0277-5387/

or diethenyl linker at the pyrrole-β position and a carboxylate binding group to give the device efficiencies up to 7.1% [26]. Grätzel and co-workers have redesigned and reported a porphyrin sensitizer (YD2-o-C8) based on D–π–A concept [27]. The new porphyrin with co-sensitization of an organic dye (Y123) using cobalt redox electrolyte attained a power conversion efficiency of 12.3%. Recently, same group has further re-designed the porphyrin macrocycle by introducing benzenethiadiazole group with an efficiency of 13% [28], which is superior to those developed based on Ru(II) polypyridyl complexes and becomes a new milestone in this area. The high efficiency of porphyrins sensitizers is probably due to the bathochromic shift of absorption and minimization of charge recombination. The bathochromic shift of absorption spectra of porphyrins were also done by introduction of hetero aromatic molecules like thiophene and furan either at *meso*-phenyl or at pyrrole-β position [29,30]. However, introducing the similar hetero aromatic groups either at *meso*-phenyl or at pyrrole-β position of porphyrin macrocycle and compare their photovoltaic performance was not reported in the literature to the best of our knowledge.

In the present work, we have synthesized a series of four new porphyrin based sensitizers having a furan hetero aromatic ring between the porphyrin macrocycle and anchoring group either at *meso*-phenylor at pyrrole-β position of porphyrin. The porphyrin macrocycle acts as donor, furan hetero cycle acts as π-spacer and either cyanoacetic acid or malonic acid group acts as acceptor. They are 5,10,15,20-tris(4-methylphenyl)Zinc(II)porphyrinato-furan-2-(2-cyano-2-yl-acrylic acid)[**β-Zn-CAA**], 5,10,15,20-tris(4-methylphenyl)Zinc(II)porphyrinato-furan-2-(2-yl-methylene malonic acid) [**β-Zn-MA**], 5-(5-(4-Phenyl)-10,15,20-tris(4-methylphenyl) Zinc (II) porphyrinato)-furan-(2-cyano-2-yl-acrylic acid [***meso*-Zn-CAA**] and 5-(5-(4-Phenyl)-10,15,20-tris(4-methylphenyl) Zinc (II) porphyrinato)-furan-(2-yl-methylene malonic acid) [***meso*-Zn-MA**]. The structure of the photosensitizers is shown in Schemes 1 and 2. All four compounds were characterized by UV–Visible, ^{1}H NMR, MALDI-MS, and fluorescence spectroscopies as well as cyclic voltammetry and their device efficiency was evaluated by using I^-/I_3 redox couple. Theoretical study of the compounds has also been performed by the first-principles calculations.

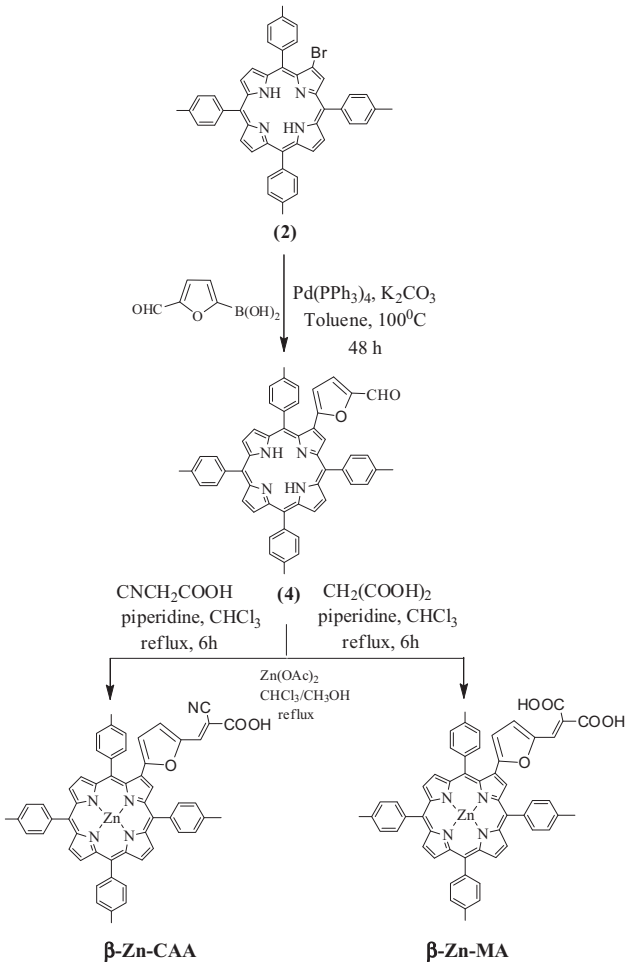

Scheme 1. Synthetic Scheme of β-Zn-CAA and β-Zn-MA.

2. Experimental

2.1. Materials

Analytical reagent grade solvents and reagents were used for synthesis, and distilled laboratory grade solvents were used for chromatography. Milli-Q water was used for synthetic and purification purpose. Dry toluene, chloroform and dichloromethane were prepared by argon-degassed solvent through activated alumina columns. N_2 (oxygen-free) was passed through a KOH drying column to remove moisture.

ACME silica gel (100-200 mesh) was used for column chromatography and thin-layer chromatography was performed on Merck-precoated silica gel 60-F_{254} plates. Either gravity or flash chromatography was used for compound purification. Where a dual solvent system was used, gradient elution was employed, and the major band was collected. All porphyrin reactions were carried out under nitrogen or argon atmosphere using dry degassed solvents, and the apparatus was shielded from ambient light.

2.2. Synthesis

The compounds 5,10,15,20-tetratolyl porphyrin (H_2TTP), 5,10,15,20-tetratolyl porphyrinato zinc(II) (ZnTTP), 2-bromo-5,10,15,20-tetratolyl porphyrin (**1**), and 5-(4-bromophenyl)-10,15,20-tritolyl porphyrin (**2**) were synthesized according to the reported procedures in the literature [31].

2.2.1. Synthesis of 2-(5-formylfuran)-5,10,15,20-tetra(tolyl) porphyrin (*3*)

1 (35 mg, 0.047 mmol), 5-formyl furan-2-boronic acid (26.32 mg, 0.188 mmol), K_2CO_3 (52.61 mg, 0.380 mmol), Palladium tetrakis (triphenyl phosphine), (5.42 mg, 0.0047 mmol) in a dried single neck round bottom flask, evacuated with nitrogen and then refilled. To this 20 ml of toluene was added and the resulting reaction mixture was heated to 90–100 °C for 48 h. The solvent was removed under vacuum and obtained solid was washed three times with $CHCl_3$, filtered, dried over anhydrous Na_2SO_4 and solvent removed under vacuum. The brown colour crude material obtained was subjected to silica gel column chromatography and eluted with $CHCl_3$. The second brown colour band was the desired compound in 62% yield. *Anal.* Calc. for $C_{52}H_{38}N_4O_2$ (764.91): C, 83.22; H, 5.27; N, 7.32. Found: C, 83.21; H, 5.25; N, 7.30%. ^{1}H NMR: 9.49 (s, 1 H), 8.96–8.78 (m, 7 H), 8.11 (d, 8 H), 7.56–7.54 (m, 8 H), 7.10 (d, 1 H, J = 3.77 Hz), 6.40 (d, 1H, J = 3.77 Hz), 2.70 (S, 12 H), −2.61 (s, 2 H). ESI MS ($C_{53}H_{40}N_4O_2$) m/z: 765 (M+1), 766 (M+2).

2.2.2. Synthesis of β-Zn-CAA

3 (200 mg, 0.24 mmol) and cyanoacetic acid (107.53 mg, 1.265 mmol) was dissolved in 100 ml of $CHCl_3$. To this piperidine

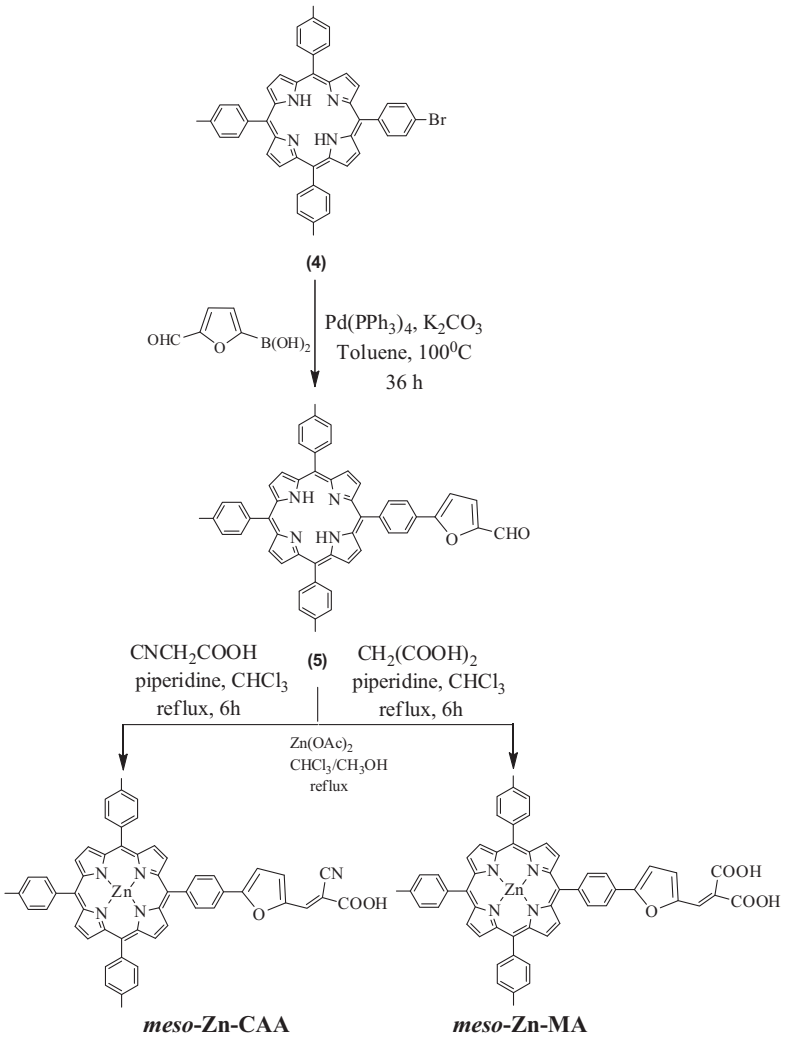

Scheme 2. Synthetic Scheme of *meso*-Zn-CAA and *meso*-Zn-MA.

(0.956 ml, 9.18 mmol) was added drop-wise and the reaction mixture was heated to reflux for 5 h. After cooling to room temperature, the reaction mixture was washed with water and 0.1 M HCl. The organic layer was dried over anhydrous Na_2SO_4. The solvent was removed under vacuum and the residue was subjected to silica gel column chromatography and eluted with methanol/dichloromethane (95:5% v/v) mixture as eluent. The solvent front running brown colour band was collected. The obtained free-base compound was then subjected to Zinc metallation using $Zn(OAc)_2$ and $CHCl_3$/Methanol to get the corresponding zinc derivative in 75% yield. *Anal.* Calc. for $C_{56}H_{39}N_5O_3Zn$ (895.33): C, 75.12; H, 4.39; N, 7.82. Found: C, 75.15; H, 4.40; N, 7.80%. ESI MS ($C_{56}H_{39}N_5O_3Zn$) m/z: 894 (M^+), 917 ($M+Na^+$). ^1H NMR: 8.99 (s, 1 H), 8.87–8.75 (m, 7 H), 8.10–7.90 (m, 8 H), 7.97 (d, 2 H), 7.68–7.60 (m 8 H), 2.69 (s, 12 H). FT IR (KBr, λ_{max}/cm^{-1}): 2210 (–CN). UV–Vis(λ_{abs}, nm) in THF: 425 (5.03), 554 (4.06), 607 (3.90).

2.2.3. Synthesis of β-Zn-MA

This compound was synthesized by an analogous manner to that described above for the synthesis of β-*Zn-CAA*, but only the difference is that by replacing cyanoacetic acid with malonic acid. *Anal.* Calc. for $C_{56}H_{39}N_5O_3Zn$ (914.33): C, 73.56; H, 4.41; N, 6.13. Found: C, 73.55; H, 4.40; N, 7.10%. ESI MS ($C_{56}H_{40}N_4O_5Zn$) m/z: 912 (M−2), 849 (M^+−Zn). FT IR (KBr, ν_{max}/cm^{-1}): 1615 (C=O). UV–Vis (λ_{abs}, nm) in THF: 429 (5.11), 564 (4.33), 607 (4.21).

2.2.4. 5-(5-(4-Phenyl)-10,15,20-tris(4-methylphenyl)porphyrin)-furan-2-carbaldehyde (*4*)

This compound was synthesized by an analogous manner to that described above for the synthesis of **3**, but by replacing **1** with **2**. *Anal.* Calc. for $C_{52}H_{38}N_4O_2$ (750.88): C, 83.18; H, 5.10; N, 7.46. Found: C, 83.20; H, 5.12; N, 7.50%. ESI MS ($C_{52}H_{38}N_4O_2$) m/z: 756 (M+). ^1H NMR: 9.8 (s, 1H), 8.84–8.78 (m, 8H), 8.31 (d, 2H), 8.10–8.08 (m, 8H), 7.90 (d, 1H), 7.81 (d, 1H, J = 8.12 Hz), 7.55 (d, 6H), 2.72 (s, 9H), −2.76 (s, 2H).

2.2.5. Synthesis of Meso-Zn-CAA

This compound was synthesized by an analogous manner to that described above for the synthesis of **β-Zn-CAA**, but by replacing **3** with **4**. *Anal.* Calc. for $C_{55}H_{37}N_5O_3Zn$ (881.30): C, 74.96; H, 4.23; N, 7.95. Found: C, 74.92; H, 4.20; N, 7.90%. ESI MS ($C_{55}H_{37}N_5O_3Zn$) m/z: 883 (M+3), 903 ($M+Na^+$). ^1H NMR: 8.88–8.54 (m, 8H), 8.30–8.17 (m, 3H), 8.1–7.8 (m, 8H), 7.64–7.33 (m, 8H), 2.72 (s, 9H). UV–Vis (λ_{abs}, nm) in THF: 423 (5.12), 558 (4.40), 597 (3.89).

2.2.6. Synthesis of Meso-Zn-MA

This compound was synthesized by an analogous manner to that described above for the synthesis of **β-Zn-MA**, but by replacing cyanoacetic acid with malonic acid. *Anal.* Calc. for $C_{55}H_{38}N_4O_5Zn$ (900.30): C, 73.37; H, 4.25; N, 6.22. Found: C, 73.40; H, 4.22; N, 6.20%. ESI MS ($C_{55}H_{38}N_4O_5Zn$) m/z: 901 (M+1), 903 (M+2), 923 ($M+Na^+$). UV–Vis (λ_{abs}, nm) in THF: 424 (5.13), 556 (4.18), 598 (4.02).

2.3. Characterization methods

The UV–Visible spectra were recorded with a Shimadzu model UV-3600 spectrophotometer for 1×10^{-6} M (porphyrin Soret band) and 5×10^{-5} M (porphyrin Q bands) solutions in THF solvent. Steady state fluorescence spectra were recorded using a Spex model Fluorolog-3 spectrofluorometer for solutions having optical density at the wavelength of excitation (λ_{ex}) ≈ 0.11. The fluorescence quantum yields (ϕ) were estimated by integrating the fluorescence bands 5,10,15,20-tetratolyl porphyrinato zinc(II) ([ZnTPP]) ($\phi = 0.036$ in CH_2Cl_2) as the standards [32]. Time-resolved fluorescence measurements have been carried out using HORIBA jobin yvon spectrofluorometer. Briefly, the samples were excited at 370 nm and the emission was monitored at 700 nm, in all unsymmetrical phthalocyanines. The count rates employed were typically 10^3–10^4 s^{-1}. Deconvolution of the data was carried out by the method of iterative reconvolution of the instrument response function and the assumed decay function using DAS-6 software. The goodness of the fit of the experimental data to the assumed decay function was judged by the standard statistical tests (*i.e.*, random distribution of weighted residuals, the autocorrelation function and the values of reduced χ^2).

2.4. Dye-sensitized solar cell fabrication

The DSSCs were made using a procedure similar to the one reported previously [33,34]. The TiO_2 electrode of 9 μm of transparent layer (TiO_2 paste DSL 18NR-T, Dyesol) and 6 μm of scatter layer (TiO_2 paste DSL 18NR-AO, Dyesol) was screen printed onto FTO substrate (TEC15, Pilkington, UK). Prior to the deposition of TiO_2, FTO substrates were treated with 40 mM $TiCl_4$ at 70 °C for 30 min by chemical bath deposition. The deposited films were annealed in air at 325 °C for 5 min, at 375 °C for 5 min, and at 450 °C for 15 min, and finally, at 500 °C for 15 min before having another $TiCl_4$ treatment (40 mM at 70 °C for 30 min). The electrodes were annealed at 450 °C for 30 min in air. The electrodes were then sensitized with a 0.2 mM solution dye molecules in THF solvent for 20 h. Platinised counter electrodes were made with transparent platinum paste (Plastisol T/SP, Solaronix SA) on FTO substrates, and heated at 450 °C for 15 min. The counter and working electrodes were then sealed together using a hot melt polymer film (Surlyn, Solaronix, SA) gas ket, before a solution of 0.05 M I_2, 0.1 M LiI,0.6M1-butyl-3-methylimidazoliumiodide and 0.5 M tertbutylpyridine in a 85:15 volume ratio of acetonitrile and valeronitrile was introduced into the cell through a pre-drilled hole in the counter electrode. The device was then sealed with the hot melt polymer and glass cover.

2.5. Theory

In the design of this series of porphyrin sensitizers, the introduction of furan group is expected to be extended π-conjugation, which broadens and red-shifts absorption spectra. The studies were performed using the density functional theory (DFT) [35,36] approach implemented in GAUSSIAN *09* [37], while the results were visualized through *Gabedit* [38] and *GaussView* [39]. We have considered the dye molecules as shown in Schemes 1 and 2. DFT and time depended DFT (TD-DFT) calculations at B3LYP/6-31G* level of theory were used for the electronic structure properties of the mentioned materials; further detail of this method can be found in our previous work [40–43]. Theoretical study of the porphyrin macrocycle which acts as donor, furan hertero cycle as π-spacer and either cyanoacetic acid or malonic acid group acts as acceptor are investigated with electronic properties such as frontier molecular orbitals (HOMO–LUMO), and UV–Vis spectral analysis. Charge analysis are simulated at natural bonding orbital (NBO) and Mullikan charge analyses. THF was used a solvent medium, using polarized continuum model (PCM) for the UV–Vis spectra and ΔSCF energy gap (optical gap) at TD-DFT-B3LYP/6-31G* level of theory.

3. Results and discussion

3.1. Design and synthesis

The broadening of the absorption of the sensitizer can improve the conversion efficiency. It can be achieved by introducing extended π-conjugation in the molecular structure of the sensitizer. The Q-band absorption bands of prophyrins are broadend by introduction of hetero aromatic molecules like thiophene [29,30]. Here, we have achieved the broadening of absorption porphyrin macrocycle with furan hetero aromatic molecule. The new sensitizers based on porphyrin-furan conjugates have been synthesized as per the Schemes 1 and 2. The purification of all the compounds were done by silica gel column chromatography and followed by recrystallization. All these sensitizers were characterized by CHN analysis, UV–Visible, ^{1}H NMR, Mass and fluorescence spectroscopies (both steady-state & life-time) as well as cyclic voltammetry. The elemental analyses data presented in experimental sections were found to be satisfactory. Each of the Mass spectrum consists of molecular ion peak ascribe to the presence of corresponding porphyrin sensitizer (*see* Section 2).

3.2. Optical and electrochemical properties

The electronic absorption spectra of these porphyrin based sensitizers were recorded in THF solution. Fig. 1 shows the absorption spectra of β-Zn-CAA and *meso*-Zn-CAA, while their TD-DFT simulated UV–Vis spectra are given in Fig. 2. Both of the theoretical and experimental wavelengths of maximum absorbance (λ_{max}) and molar extinction coefficient (ε) values of these porphyrin-furan conjugates as obtained from UV–Vis studies, are summarized in Tables 1 and 2, respectively. The absorption spectra of these

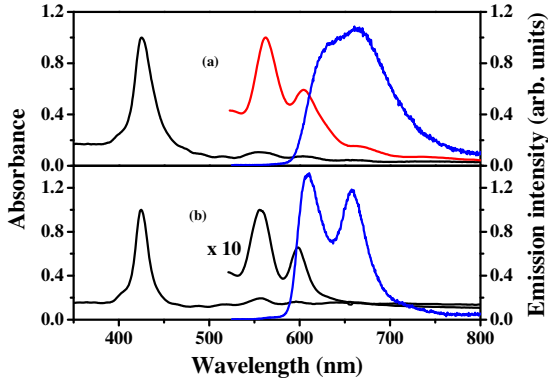

Fig. 1. (a) UV–Visible absorption spectra of (—) & emission spectrum of (—) β-Zn-CAA. (b) UV–Visible absorption spectra of (—) & emission spectrum of (—) *meso*-Zn-CAA in THF solvent.

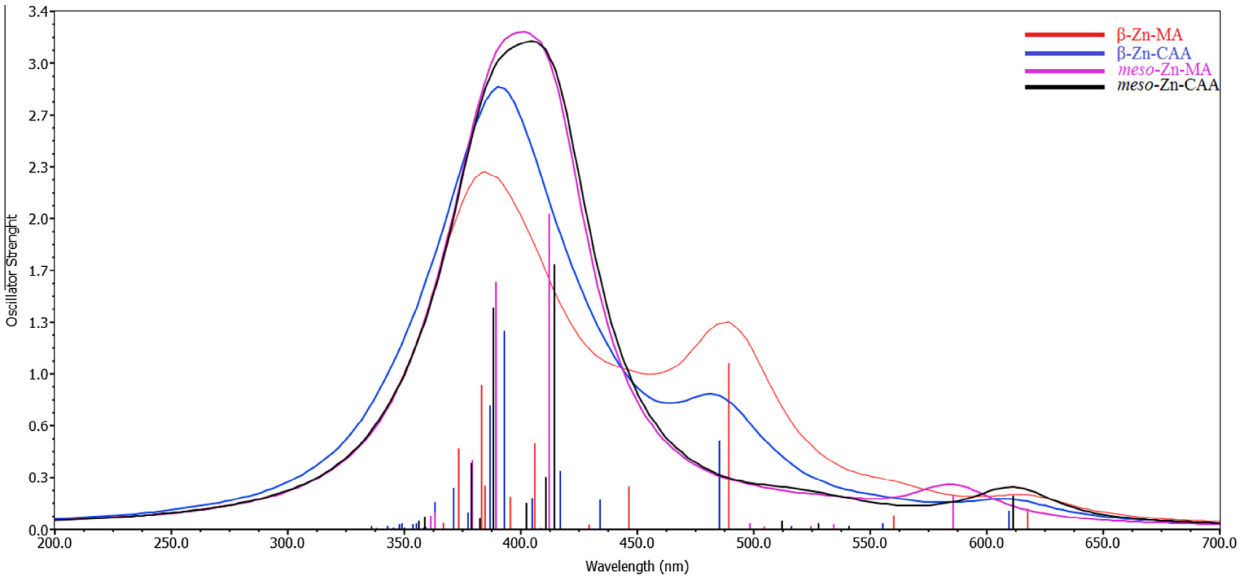

Fig. 2. TD-DFT simulated UV–Vis spectra of Zn Porphyrin-Furan dyes.

porphyrin-furan conjugates in THF solution shows an intense soret band between 420-430 nm and two less intense Q-bands between 500 to 625 nm due to π–π^* absorption of the conjugated macrocycle. Observed and simulated UV–Vis spectra has strong correlation among their absorption band peaks as can be seen from Figs. 1 and 2 and Table 1 and 2. Both Soret and Q-bands are red-shifted (5-10 nm in case of pyrrole-β substituted and 3-5 nm in case of *meso*-phenyl substituted porphyrins) in comparison with its parent porphyrin *i.e.,* ZnTTP. The shift in absorption bands are probably due to the electron with-drawing nature of furan substituent. A similar red shift was also observed in other pyrrole-β and *meso*- substituted porphyrins [29,30,44,45].

Fig. 1 also shows the emission spectra of β-Zn-CAA and meso-Zn-CAA in THF solvent at room temperature and the corresponding emission maxima & quantum yield data are presented in Table 1. The emission maxima (Table 1) are independent of the excitation wavelength between 400 and 600 nm, and spectra shown characteristic vibronic bands between 610 and 675 nm similar to those reported other zinc porphyrins. The emission maxima of all four porphyrin-furan conjugates are red-shifted in comparison with its constituent ZnTTP. The quantum yields are slightly reduced in comparison with ZnTTP probably due to the substituent effect of furan group on porphyrin macrocycle. The excitation spectrum obtained by exciting emission maximum at 660 nm exhibit an intense Soret and Q-bands that corresponds to the ground state absorption spectra, indicating the presence of single emitting species in each case. Based on absorption and emission, the singlet excited state [$E_{0\text{-}0}$] energy of β-Zn-CAA,β-Zn-Ma, *meso*-Zn-CAA and

Table 2
TD-DFT calculated electronic excitations (λ_{max}) and optical gap of Zn porphyrin-furan dyes.

Species	Maximum excitation	Oscillator strength	Electronic transition	Optical Gap (eV)
β-Zn-MA	617	0.13	$\pi \rightarrow \pi^*$	2.00
β-Zn-CAA	609	0.11	$\pi \rightarrow \pi^*$	2.03
meso-Zn-MA	585	0.22	$\pi \rightarrow \pi^*$	2.11
meso-Zn-CAA	611	0.22	$\pi \rightarrow \pi^*$	2.02

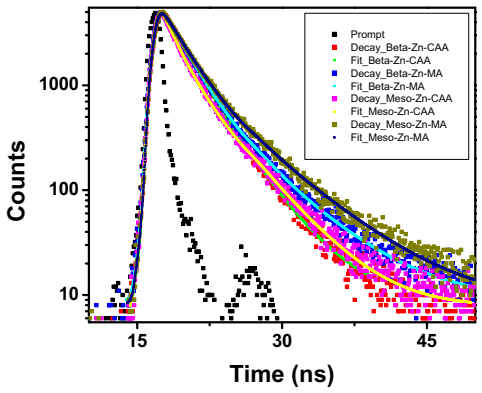

Fig. 3. Fluorescence decay of all four porphyrin-furan conjugates.

Table 1
Absorption, steady state and time resolved emission data.[a]

Sample	λ_{max}, nm, log ε/M^{-1} cm^{-1}[b]	λ_{em}, (ϕ)[c]	τ_1 (*ns*)	τ_2 (*ns*)
Beta-Zn-CAA	425 (5.03), 554 (4.06), 607 (3.90)	664 (0.032)	1.04 (62)	1.84 (38)
Beta-Zn-MA	429 (5.11), 564 (4.33), 607 (4.21)	660 (0.026)	1.08 (69)	2.67 (31)
Meso-Zn-CAA	423 (5.12), 558 (4.40), 597 (3.89)	659 (0.027)	1.97 (52)	6.73 (48)
Meso-Zn-MA	424 (5.13), 556 (4.18), 598 (4.02)	657 (0.030)	1.02 (57)	2.80 (43)

[a] Solvent THF.
[b] Error limits: λ_{max}, ±1 nm, log ε, ±10%.
[c] Error limits: λ_{em} = ±1 nm.

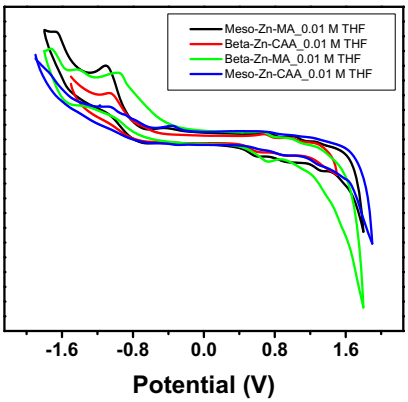

Fig. 4. Cyclic and Differential Pulse Voltammogrammes in THF and 0.1 M TBAP.

β-Zn-CAA and *meso*-Zn-MA are found to be 2.05, 2.05, 2.06, and 2.07 eV, respectively. We also simulated this singlet excited state (optical band gap) energy at ΔSCF method, which has excellent matching as can be seen from Table 2. The simulated optical band gap of β-Zn-MA is 2.0 eV,β-Zn-CAA has 2.03 eV, *meso*-Zn-MA has 2.11 eV and *meso*-Zn-CAA has 2.02 eV optical band gap.

No emission spectra are observed for the porphyrin-furan conjugates adsorbed onto 6 μm thick TiO_2 layer as a consequence of electron injection from excited singlet state of porphyrin into the conduction band of TiO_2. Fig. 3 illustrates fluorescence decay curves of all four investigated compounds in THF solvent. The singlet excited life-time of all four porphyrin-furan conjugates were measured in THF solvent and found 1.04, 1.08, 1.97 & 1.02 ns for β-Zn-CAA, β-Zn-Ma, *meso*-Zn-CAA and *meso*-Zn-MA, respectively. In all these cases the excited state life-time quenched when adsorbed onto 2 μm thick TiO_2 layer.

With a view to evaluate the HOMO–LUMO levels of porphyrin-furan conjugates, we performed the electrochemistry by using cyclic and differential pulse voltammetric techniques in THF solvent. Fig. 4 shows the cyclic voltammograme of β-Zn-CAA and the corresponding data are presented in Table 3. Analysis of Fig. 4 and Table 3 it is evident that each porphyrin-furan conjugate undergoes two oxidations and two reductions under the experimental conditions employed in this study. Wave analysis suggested that while the first two oxidation and first two reduction processes represent reversible (i_{pc}/i_{pa} = 0.9–1.0) and diffusion controlled ($i_{pc}/\upsilon^{1/2}$ = constant in the scan rate (υ) range 50–500 mV/s) one-electron transfer (ΔE_P = 60–70 mV; ΔE_P = 65 ± 3 mV for Fc^+/Fc couple) reactions, left over electrode processes are either quasi-reversible (i_{pc}/i_{pa} = 0.6–0.8 and ΔE_P = 80–150 mV) or irreversible under similar experimental conditions. Analysis of the data given in Table 1 reveals that the redox potentials of these porphyrin-furan conjugates are not altered when compared to its reference compound. Each porphyrin-furan conjugate undergoes oxidation at 0.73, 0.69, 0.64, and 0.63 V vs. SCE generating π-cation for β-Zn-CAA, β-Zn-Ma, *meso*-Zn-CAA and *meso*-Zn-MA, respectively.

Table 3
Electrochemical data.

Sample	$E_{1/2}$oxd (V)[a]	$E_{1/2}$red (V)[a]	$E_{0\text{-}0}$ (eV)[b]	E^*_{oxd} (V)[c]	$\Delta G_{inj.}$ (V)	$\Delta G_{reg.}$ (V)
Beta-Zn-CAA	0.73	−1.58	2.05	−1.32	−0.82	0.23
Beta-Zn-MA	0.69	−1.56	2.05	−1.36	−0.86	0.19
Meso-Zn-CAA	0.64	−1.59	2.06	−1.42	−0.99	0.07
Meso-Zn-MA	0.63	−1.58	2.07	−1.44	−0.94	0.13

$E_{0\text{-}0}$ = HOMO–LUMO gap calculated from the intersection of the absorption and fluorescence spectra.
$\Delta G_{inj.}$ = driving force for electron injection from the LUMO of the dye to the conduction band of TiO_2.
$\Delta G_{reg.}$ = driving force for regeneration of the oxidized dye from the redox electrolyte.
[a] Error limits, $E_{1/2}$, ±0.03 V, 0.1 M TBAP.
[b] Error limits: ±0.05 eV. $E^*_{oxd} = E_{1/2} - E_{0\text{-}0}$.

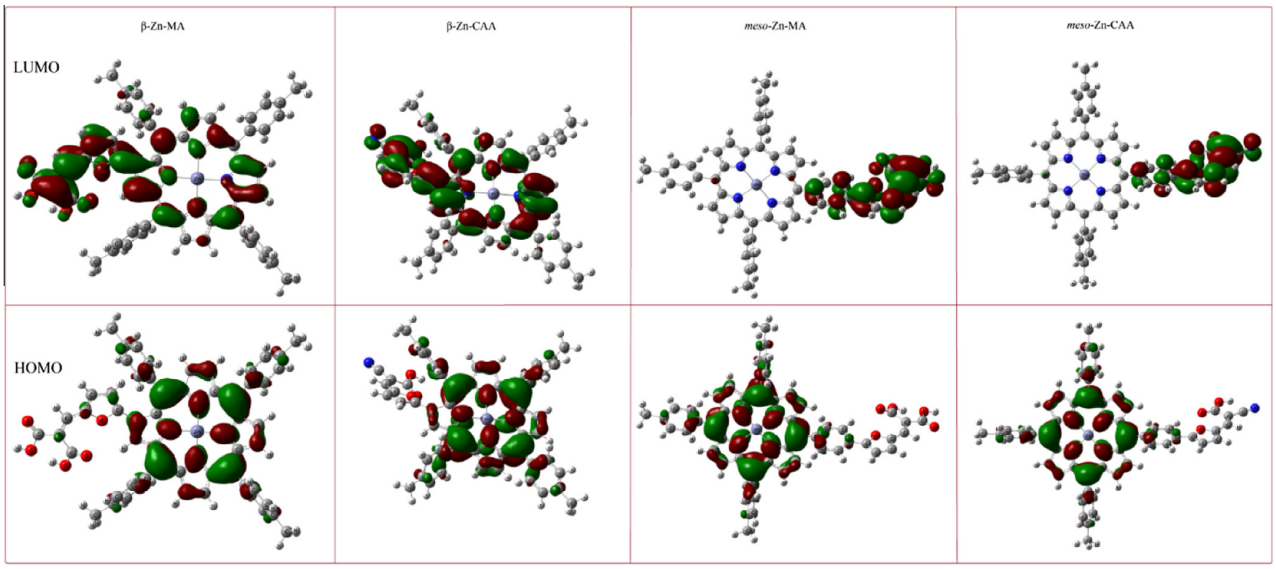

Fig. 5. Contours of HOMO and LUMO of Zn porphyrin-furan dyes.

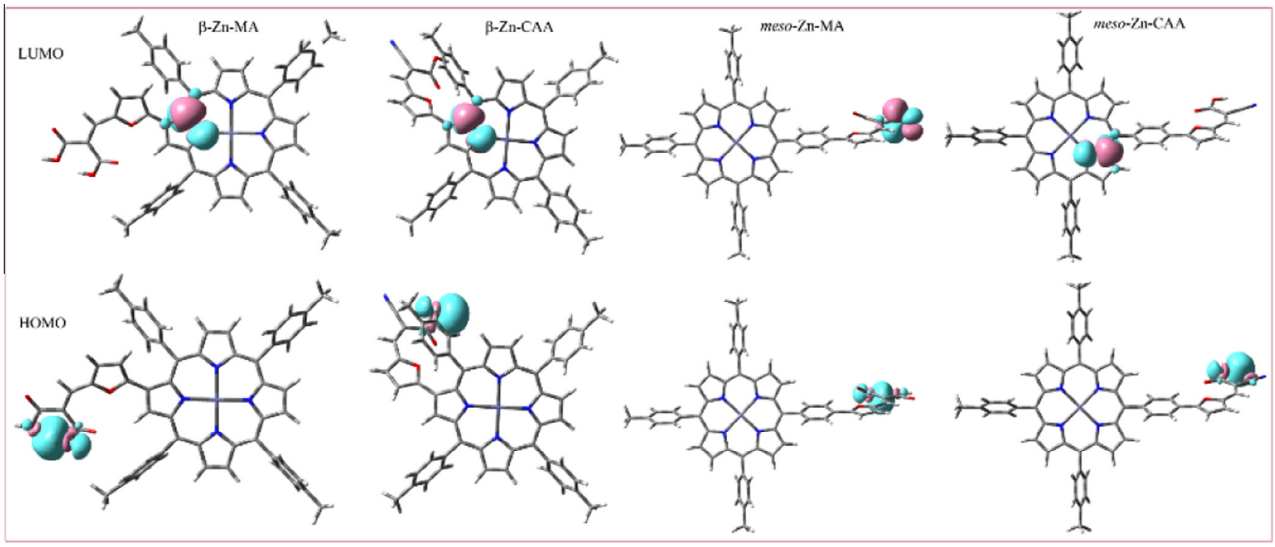

Fig. 6. Contours of occupied and unoccupied NBO of Zn porphyrin-furan dyes.

With respect to dye-sensitization of wide-band-gap semiconductors, e.g. TiO_2, the oxidation potentials of porphyrin sensitizers and the $E_{0\text{-}0}$ transition energy, the energy levels of the singlet excited states (excited state oxidation potential) of β-Zn-CAA, β-Zn-Ma, *meso*-Zn-CAA and *meso*-Zn-MA −1.32, −1.36, −1.42, and −1.44, respectively. Whereas the energy level of the conduction band edge of TiO_2 is ca. −0.74 V vs. SCE [46]. This makes electron injection from the excited state of porphyrin sensitizer into the conduction band of TiO_2 thermodynamically feasible. Furthermore, the HOMO level of the porphyrins is lower than the energy level of the redox couple I^-/I_3^- (0.2 V vs. SCE) in the electrolyte, enabling the dye regeneration by electron transfer from iodide ions in the electrolyte.

The theoretical predicted frontier molecular and natural bonding orbital's (NBO) contours of these dyes are shown in Figs. 5 and 6. Topmost HOMO is strongly contributed by the N 2*p* states whereas the lowest LOMO is strongly contributed by C 2*p*-like states slightly hybridized with O 2*p* and C 2*p* states. Most contribution to the highest HOMO and lowest LUMO states are coming from *p* electrons whereas contribution from *s*-electrons is modest. Since the *p*–*p* electrons transitions are not allowed, very strong absorption of sunlight by the molecule is not expected. Fig. 6 displays electron localization function for the dyes. Analysis shows that the electrons are distributed around the ring, so the dye molecules can be oxidized. The electrons are localized around H, N, O, and C atoms and are located in the covalent C–C, C–O, C–Zn, C–H bonds. Although good light absorption properties of the dyes are important for high efficiency solar cells, electrical properties of the molecules, charge transfer between the molecule and TiO_2 as well as the interface are the other important factors. That might explain the reason of getting the low efficiency of the cells.

Highest electronic cloud density on the HOMO at anchoring sites of these dyes clearly predict that charge injection is favoured while the lowest one on the LUMO shows that charge recombination is prevented. From the NBO contours of all these dyes (Fig. 6), it is evident that except the *meso*-Zn-MA, the rest of them have good electron donating ability.

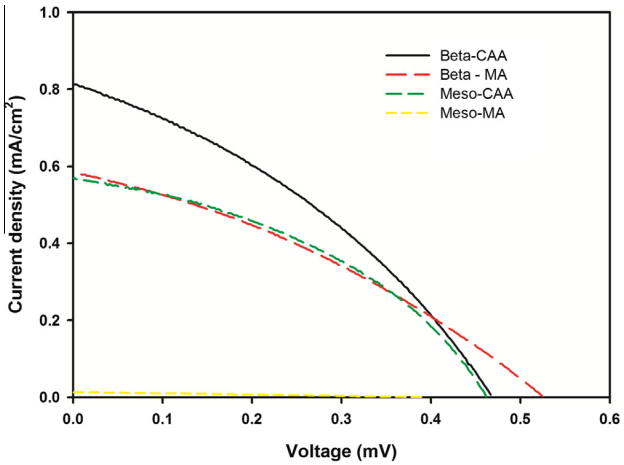

Fig. 7. J–V characteristics of DSSCs constructed with different porphyrin sensitizers under 1 sun illumination.

3.3. Photovoltaic properties

Fig. 7 shows the performance of the DSSCs of different sensitizers on the basis of their steady-state current–voltage characteristics. Table 4 summarizes the key cell parameters for DSSCs as a function of different porphyrin sensitizers. DSSC parameters are significantly influenced by the porphyrin sensitizers. The maximum conversion efficiency has been achieved for the cells sensitized with β-CAA. It shows slightly improved J_{sc} (0.813 ± 0.15 mA cm^{-2}) and V_{oc} (467 ± 10 mV) than its *meso*-CAA which shows J_{sc} (0.569 ± 15 mA cm^{-2}) and V_{oc} (462 ± 10 mV) effects in the frontier orbitals. This might be due

Table 4
Test cell data.[a]

Sensitizer	V_{oc} (mV)	J_{sc}(mA/cm^2)	ff(%)	η (%)
Beta-CAA	467 ± 10	0.813 ± 0.15	35.24 ± 0.10	0.1330 ± 0.01
Beta-MA	525 ± 10	0.584 ± 0.15	33.49 ± 0.10	0.1020 ± 0.01
Meso-CAA	462 ± 10	0.569 ± 0.15	40.42 ± 0.10	0.1060 ± 0.01
Meso-MA	391 ± 10	0.013 ± 0.15	27.38 ± 0.10	0.0013 ± 0.01

[a] Photoelectrode: TiO_2 (9 + 6 μm and 0.74 cm^2); electrolyte: 0.6 M1-butyl-3-methylimidazoliumiodide, 0.05 M I_2, 0.5 M tertbutylpyridine and 0.1 M guanidine thiocyanate in a 85:15 volume ratio of acetonitrile and valeronitrile.

to the presence of π-electron cloud at β-pyrrole position than at *meso* phenyl position. More over the sensitizers having cyanoacetic acid anchoring group showing better performance than the corresponding sensitizers having dicarboxylic acid anchoring group probably due to the presence of electron withdrawing –CN group. However, the overall conversion efficiency is less than the controlled cells made with standard N719 sensitizer (J_{sc}18.1 ± 0.15 mA cm^{-2} and V_{OC} 622 ± 10 mV) [47].

The reason for the low efficiency compared to the previously reported thiophene spacer porphyrins might be related to poor electrical conductivity of furan derivatives [30,48], offset between HOMO/LUMO of the porphyrins and valence/conduction bands of TiO_2, as well as quality of interface between them. However, one has to investigate in detail about the charge injection of present sensitizers and compare with thiophene derivatives. The detailed charge injections studies are currently under progress.

4. Conclusions

In conclusion, we have designed, synthesized and theoretically counterchecked for the first time porphyrin–furan conjugates, in which anchoring group either at *meso*-phenyl or at pyrrole-β position of a zinc porphyrin based on donor-π-acceptor approach. The newly synthesized dyes are characterized by UV–Visible, ^{1}H NMR, MALDI-MS and fluorescence spectroscopies and cyclic voltammetry. Theoretical data simulated with DFT and TD-DFT at B3LYP/6-31G* level theory has nice correlation with our experiment. It is found that this level of theory can be used for the new dyes to predict and improve their efficiency. Both optical and electrochemical properties of pyrrole-β substituted dyads are altered whereas its meso-phenyl substituted dyads are not altered, when compared to its reference zinc porphyrin. The dyads were tested in dye sensitized solar cells using I-/I_3^- redox couple. The pyrrole-β substituted porphyrins are showing better efficiency than its meso-phenyl substituted dyads. Overall the efficiency of these sensitizers are found to very low. Optical band gap, Natural bonding, and Molecular bonding orbital (HOMO–LUMO) analysis are also in favour of pyrrole-β substituted zinc porphyrins contrast to *meso*-phenyl dyads.

Acknowledgements

The authors are thankful to DST(India)-EPSRC(UK) ('APEX') programme and the EPSRC Supergen programme for financial support of this work.

References

[1] L. Giribabu, K. Sudhakar, J. Photochem. Photobiol., A 296 (2015) 11.
[2] F. D'Souza, O. Ito, Chem. Soc. Rev. 41 (2012) 86.
[3] D. Gust, T.A. Moore, A.L. Moore, Acc. Chem. Res. 42 (2009) 1890.
[4] M.-M. Yu, J. Li, W.-J. Sun, M. Jiang, F.-X. Zhang, J. Mater. Sci. 49 (2014) 5519.
[5] M.E. El-Khouly, D.K. Ju, K.-Y. Kay, F. D'Souza, S. Fukuzumi, Chem. Eur. J. 16 (2010) 6193.
[6] G. Pagona, G.E. Zervaki, A.S. Sandanayaka, O. Ito, G. Charalambidis, T. Hasobe, A.G. Coutsolelos, N. Tagmatarchis, J. Phys. Chem. C 116 (2012) 9439.
[7] C.M. Davis, K. Ohkubo, A.D. Lammer, D.S. Kim, Y. Kawashima, J.L. Sessler, S. Fukuzumi, Chem. Commun. 51 (2015) 9789.
[8] T. Ripolles-Sanchis, B.-C. Guo, H.-P. Wu, T.-Y. Pan, H.-W. Lee, S.R. Raga, F. Fabregat-Santiago, J. Bisquert, C.-Y. Yeh, E.W.-G. Diau, Chem. Commun. 48 (2012) 4368.
[9] B. Basheer, D. Mathew, B.K. George, C.P. Reghunadhan Nair, Solar Energy 108 (2014) 479.
[10] J. Kandhadi, R.K. Kanaparthi, L. Giribabu, J. Porphyrins Phthalocyanines 16 (2012) 282.
[11] L. Giribabu, P.S. Reeta, R.K. Kanaparthi, M. Srikanth, Y. Soujanya, J. Phys. Chem. A 117 (2013) 2944.
[12] F.-C. Gong, D.-X. Wu, Z. Cao, X.-C. He, Biosens. Bioelectron. 22 (2006) 423.
[13] V.A. Montes, C. Pérez-Bolívar, N. Agarwal, J. Shinar, P. Anzenbacher, J. Am. Chem. Soc. 128 (2006) 12436.
[14] M.-L. Seol, S.-J. Choi, C.-H. Kim, D.-I. Moon, Y.-K. Choi, ACS Nano 6 (2012) 183.
[15] S.V. Rao, N.K.M. Naga Srinivas, D.N. Rao, L. Giribabu, B.G. Maiya, R. Philip, G.R. Kumar, Opt. Commun. 192 (2001) 123.
[16] L. Giribabu, R.K. Kanaparthi, V. Velkannan, Chem. Rec. 12 (2012) 306.
[17] R.K. Kanaparthi, J. Kandhadi, L. Giribabu, Tetrahedron 68 (2012) 8383.
[18] H.M. Upadhyaya, S. Senthilarasu, M.-H. Hsu, D.K. Kumar, Sol. Energy Mater. Sol. Cells 119 (2013) 291.
[19] M. Urbani, M. Grätzel, M.K. Nazeeruddin, T.S. Torres, Chem. Rev. 114 (2014) 12330.
[20] T. Higashino, H. Imahori, Dalton Trans. 44 (2015) 448.
[21] B. O'Regan, M. Gratzel, Nature 353 (1991) 737.
[22] M.K. Nazeeruddin, A. Kay, I. Rodicio, R. Humphry-Baker, E. Mueller, P. Liska, N. Vlachopoulos, M. Graetzel, J. Am. Chem. Soc. 115 (1993) 6382.
[23] L. Han, A. Islam, H. Chen, C. Malapaka, B. Chiranjeevi, S. Zhang, X. Yang, M. Yanagida, Energy Environ. Sci. 5 (2012) 6057.
[24] W.M. Campbell, A.K. Burrell, D.L. Officer, K.W. Jolley, Coord. Chem. Rev. 248 (2004) 1363.
[25] J. Jasieniak, M. Johnston, E.R. Waclawik, J. Phys. Chem. B 108 (2004) 12962.
[26] W.M. Campbell, K.W. Jolley, P. Wagner, K. Wagner, P.J. Walsh, K.C. Gordon, L. Schmidt-Mende, M.K. Nazeeruddin, Q. Wang, M. Grätzel, D.L. Officer, J. Phys. Chem. C 111 (2007) 11760.
[27] A. Yella, H.-W. Lee, H.N. Tsao, C. Yi, A.K. Chandiran, M.K. Nazeeruddin, E.W.-G. Diau, C.-Y. Yeh, S.M. Zakeeruddin, M. Grätzel, Science 334 (2011) 629.
[28] S. Mathew, A. Yella, P. Gao, R. Humphry-Baker, F.E. CurchodBasile, N. Ashari-Astani, I. Tavernelli, U. Rothlisberger, K. NazeeruddinMd, M. Grätzel, Nat. Chem. 6 (2014) 242.
[29] Y. Liu, N. Xiang, X. Feng, P. Shen, W. Zhou, C. Weng, B. Zhao, S. Tan, Chem. Commun. (2009) 2499.
[30] V.A. Nuay, D.-H. Kim, S.-H. Lee, J.-J. Ko, Bull. Korean Chem. Soc. 30 (2009) 2871.
[31] J.-H. Fuhrhop, K.M. Smith, Laboratory Methods in Porphyrin and Metalloporphyrin Research, Elsevier Science & Technology, 1975.
[32] D.J. Quimby, F.R. Longo, J. Am. Chem. Soc. 97 (1975) 5111.
[33] L. Giribabu, V.K. Singh, C.V. Kumar, Y. Soujanya, P.Y. Reddy, M.L. Kantam, Sol. Energy 85 (2011) 1204.
[34] J.W. Bowers, H.M. Upadhyaya, S. Calnan, R. Hashimoto, T. Nakada, A.N. Tiwari, Prog. Photovoltaics 17 (2009) 265.
[35] H. Ullah, A.-U.-H. A. Shah, K. Ayub, S. Bilal, J. Phys. Chem. C 117 (2013) 4069.
[36] H. Ullah, A.A. Shah, S. Bilal, K. Ayub, J. Phys. Chem. C 117 (2013) 23701.
[37] M.J. Frisch, G.W. Trucks, H.B. Schlegel, G.E. Scuseria, M.A. Robb, J.R. Cheeseman, G. Scalmani, V. Barone, B. Mennucci, G.A. Petersson, et al., Gaussian 09, Rev. D. 0.1, Gaussian Inc, Wallingford, CT, 2013.
[38] Allouche, A.R. Gabedit, http://gabedit.sourceforge.net, 2011.
[39] R. Dennington, T. Keith, J.G. Millam, Semichem Inc., Shawnee Mission KS, 2008.
[40] H. Ullah, A.-U.-H. A. Shah, S. Bilal, K. Ayub, J. Phys. Chem. C 118 (2014) 17819.
[41] H. Ullah, K. Ayub, Z. Ullah, M. Hanif, R. Nawaz, S. Bilal, Synth. Met. 172 (2013) 14.
[42] S. Bibi, H. Ullah, S.M. Ahmad, A.-U.-H. Ali Shah, S. Bilal, A.A. Tahir, K. Ayub, J. Phys. Chem. C 119 (2015) 15994.
[43] M. Kamran, H. Ullah, A.S. Anwar-ul-Haq, S. Bilal, A.A. Tahir, K. Ayub, Polymer 72 (2015) 30.
[44] L. Giribabu, C.V. Kumar, P.Y. Reddy, J. Porphyrins Phthalocyanines 10 (2006) 1007.
[45] P. Silviya Reeta, J. Kandhadi, G. Lingamallu, Tetrahedron Lett. 51 (2010) 2865.
[46] A. Hagfeldt, M. Graetzel, Chem. Rev. 95 (1995) 49.
[47] P.S. Reeta, L. Giribabu, S. Senthilarasu, M.-H. Hsu, D.K. Kumar, H.M. Upadhyaya, N. Robertson, T. Hewat, RSC Adv. 4 (2014) 14165.
[48] S.J. Lind, K.C. Gordon, S. Gambhir, D.L. Officer, Phys. Chem. Chem. Phys. 11 (2009) 5598.